

Numerical investigation of crystal growth in a vertical Bridgman configuration using a mushy region model

B. BARVINSCHI, P. BARVINSCHI*

Faculty of Physics, West University of Timisoara, Bd. V. Parvan 4, 300223 Timisoara, Romania

This paper considers an axisymmetric numerical model developed in COMSOL Multiphysics for the simulation of the directional solidification of a melt in an idealized vertical Bridgman configuration. The solidification of the melt, including the convection and conduction heat transfer with mushy region phase change, is modeled using a slightly modified version of a method presented by Voller and Prakash [1]. Using different thermal conditions the model was applied for the study of the effect of the axial thermal gradients and the flow in the melt on the solid-liquid interface deflection and shape, during the solidification of InSb and respectively CaF_2 melts.

(Received February 23, 2015; accepted March 19, 2015)

Keywords: Computer simulation; Bridgman technique; Mushy region; Interface shape

1. Introduction

The Bridgman growth process is one of the important methods for growing high quality II – VI and III – V semiconductors, halide and chalcogenide crystals, and a number of oxides for scintillation or laser applications [2]. In the vertical Bridgman technique the charge material is introduced in a crucible (ampoule) placed in a furnace; by heating the furnace and controlling a vertical (axial) thermal gradient the material is melted. The controlled solidification is obtained by cooling down the furnace, or by pulling down the crucible, or both. The Stockbarger variant uses a furnace made up of two heating elements separated by an adiabatic zone.

The most important process parameters in the vertical Bridgman method are i) the thermal properties of the furnace, and ii) the crucible design (shape and anisotropic properties of the ampoule material). The thermal properties of the furnace may be varied with time during the crystal growth and so the control of the crystal – melt interface shape and the growth rate can be difficult. It is known that the growth rate and the shape of the crystal – melt interface during the growth process influence the defect structure in the final crystal; for example, a flat or a slightly convex interface is desirable for growing single crystals with a low density of defects. In order to better understand how to control the shape of the solidification interface we can do experiments or we can perform numerical simulations. Because doing experiments could be time consuming and difficult, performing numerical simulations is a good choice for providing useful information for the system operation and design. Crystal growth is a transient process and its modeling requires the solution of a set of time-dependent partial differential equations. There are numerous computational studies devoted to the Bridgman crystal growth method, both in the steady-state approximation [3-9], and in the transient case [9-16]. We already proposed a steady-state model and obtained some numerical results for the coupled heat and fluid dynamics in the vertical Bridgman solidification of InSb [17]. In the present paper we extend our previous

model by using a time dependent step type temperature distribution applied on the outer wall of the crucible, in a such a way that the actual model corresponds to a pseudo-transient solidification. The influence of the thermal gradients, the flow in the melt and the pulling rate on the crystal-melt interface shape during the solidification of CaF_2 and InSb is studied. Numerical calculations have been performed with the commercial finite element software COMSOL Multiphysics.

2. Model description and implementation

2.1 Growth configuration

The geometrical configuration of the charge, crucible and furnace is shown in Fig. 1. In the axisymmetric model described here the cylindrical coordinate system has its origin at the center of the flat bottom of the crucible. The InSb charge is placed in a silica crucible (90 mm in length, having 5.5 mm inner radius and 6.5 mm outer radius). The crucible containing the CaF_2 charge is made from a material as in Ref. [16], with the properties listed in Table 1.

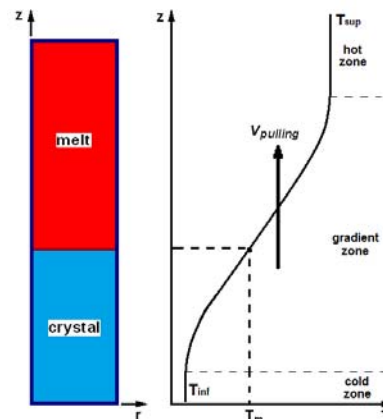


Fig. 1. Schematic diagram of the vertical Bridgman system.

The crucible is placed in an idealized Bridgman system with a three-zone furnace (Fig. 1): a gradient zone is located between a cold zone and a hot one, these ones being maintained at constant temperatures T_{inf} and T_{sup} respectively. Solidification can be controlled by changing the furnace temperature distribution with time. For example, in our simulations we use a time dependent temperature distribution on the vertical outer boundary of the crucible that can be described by a smooth step function given by:

$$T_{ext}(z, t) = T_{inf} + (T_{sup} - T_{inf}) \cdot Heav(z - z_m; \Delta z) \quad (1)$$

where t is the time, $z_m = z_0 + v_{pulling} \cdot t$, and $v_{pulling}$ is the pulling rate. The function $Heav(z - z_m; \Delta z)$ appearing in Eq. (1) is a smooth Heaviside function defined as:

$$Heav(z - z_m; \Delta z) = 0.5 \left[1 + \tanh\left(\frac{z - z_m}{\Delta z}\right) \right] \quad (2)$$

such that Δz is the half width of the gradient zone and z_m is the middle point of this interval. The temperature distribution given by Eq. (1) corresponds to a pseudo-transient solidification. The thermal gradient is then given by $(T_{sup} - T_{inf}) / (2\Delta z)$. In our simulations the initial position of the step profile in Eq. (1) is taken to be $z_0 = 0.04$ m and for the transition width Δz we consider the values 0.01 m, 0.02 m, 0.03 m, and 0.04 m respectively.

2.2 Governing equations

2.2.1 Fluid flow

The flow of the melt is modeled using the Navier-Stokes equations for incompressible laminar flow:

$$\rho \frac{\partial \mathbf{u}}{\partial t} + \rho (\mathbf{u} \cdot \nabla) \mathbf{u} = \nabla \cdot \left[-p \mathbf{I} + \eta (\nabla \mathbf{u} + (\nabla \mathbf{u})^T) \right] + \mathbf{F} \quad (3)$$

$$\nabla \cdot \mathbf{u} = 0, \quad (4)$$

In these equations \mathbf{u} denotes the velocity, ρ the density, p the pressure and η the dynamic viscosity. As it will be described in the following sections the interface between the melt and the solid is treated by using an Eulerian approach in a fixed grid [1].

The source term \mathbf{F} in Eq. (3) includes the volumetric buoyancy force and an additional term used to model the solidification. The volumetric buoyancy force is written in the Boussinesq approximation:

$$\mathbf{F}_{buoyancy} = \rho (T_{ref}) \beta \mathbf{g} (T - T_{ref}) \quad (5)$$

where β is the volumetric thermal expansion coefficient, \mathbf{g} is the gravitational acceleration, and T_{ref} is a reference temperature. The other additional term in \mathbf{F} will be detailed in the following section.

2.2.2 Solidification

The solidification model is based on that proposed initially by Voller and Prakash [1] and slightly modified by Marin [18]. In the modified model the heat equation is written in terms of temperatures rather than enthalpy, as in the original one:

$$\rho C_p \left(\frac{\partial T}{\partial t} + \mathbf{u} \cdot \nabla T \right) - \nabla \cdot (k \nabla T) = 0 \quad (6)$$

where T is the temperature, k the thermal conductivity, and C_p the heat capacity. Equation (6) is valid for the solid crystal, the melt and also for the wall of the crucible (where the convection term is suppressed).

A new feature of our model is to take into account the dependence of the density and thermal conductivity on the temperature, for the InSb and CaF₂ charges, by using the following equations:

$$\rho(T) = \rho_S \pm |\rho_L - \rho_S| \cdot Heav(T - T_m; \Delta T) \quad (7)$$

$$k(T) = k_S \pm |k_L - k_S| \cdot Heav(T - T_m; \Delta T) \quad (8)$$

where the subscripts S and L indicate the solid and liquid phases respectively, T_m is the melting point temperature, and ΔT is the half width of the temperature transition interval between the solid and liquid phases (i.e. $2\Delta T$ is the width of the mushy region). The function $Heav(T - T_m; \Delta T)$ in Eqs. (7) and (8) is a smooth Heaviside function having the same analytical form as given in Eq. (2).

To account for the latent heat related to the phase transition, in Eq. (6) we use a modified heat capacity:

$$C_p(T) = C_{pS} + |C_{pL} - C_{pS}| \cdot Heav(T - T_m; \Delta T) + L\delta \quad (9)$$

where L is the latent heat of solidification and δ is a smooth delta function taking into account that the latent heat is liberated only within the range $2\Delta T$ of the temperature, in the mushy region. For this δ function we take the following Gaussian form:

$$\delta = \frac{\exp(-(T - T_m)^2 / (\Delta T)^2)}{\Delta T \sqrt{\pi}} \quad (10)$$

The assumption of the solidification model proposed by Voller and Prakash is that the fluid flow in the

transition (mushy) region, during solidification, is similar to the flow in a porous medium. In the transition region a

$$F_S(T) = \begin{cases} 1, & T > (T_m + \Delta T) \\ (T - T_m + \Delta T)/(2\Delta T), & (T_m - \Delta T) \leq T \leq (T_m + \Delta T) \\ 0, & T < (T_m - \Delta T) \end{cases}$$

where ΔT has the same meaning as in Eqs. (7) and (8). This function takes the value 0 when the temperature is below the *solidus* temperature ($T < (T_m - \Delta T)$), and equals 1 for temperatures above the *liquidus* temperature ($T > (T_m + \Delta T)$); in the transition region F_S takes values between 0 and 1. A temperature dependent porosity function is defined as:

$$B = 1 - F_S(T), \quad (12)$$

and a solidification source term must be added in the Navier-Stokes equation results:

$$\mathbf{F}_{solidification} = -A\mathbf{u} \quad (13)$$

where

$$A = \frac{C(1-B)^2}{B^3 + q}. \quad (14)$$

C and q in Eq. (14) are constants arbitrarily chosen to achieve the desired effect: no modification of the Navier-Stokes equations in the liquid region (for $T > (T_m + \Delta T)$) and $\mathbf{u} = \mathbf{0}$ in the solid region (for $T < (T_m - \Delta T)$). In the transition region the flow is governed by the Darcy law (see [1] for details). All these conditions can be achieved if C is large enough and q is small enough; in our calculations we take $C = 1 \cdot 10^8$ and $q = 1 \cdot 10^{-4}$. Internal radiation in the crystal is not considered in the present model.

2.2.3 Boundary conditions

A set of boundary conditions must be formulated for each of the governing equations in the model. For the thermal problem the boundary conditions are:

- i) Zero temperature gradient normal to the symmetry axis.
- ii) Constant temperatures T_{inf} and T_{sup} on the bottom and respectively upper surfaces of the crucible.
- iii) A smooth step temperature distribution given by Eq. (1) on the vertical outer boundary of the crucible. Taking $v_{pulling} = 0$ results in a stationary temperature distribution on this boundary.

Heat transfer from the system to the ambient by radiation and convection is not considered in the present model.

For the flow problem the *no-slip* boundary condition is imposed at the contact between the melt and the solid

solid fraction function F_S is defined as a simple linear function of temperature:

$$\begin{cases} T > (T_m + \Delta T) \\ (T_m - \Delta T) \leq T \leq (T_m + \Delta T) \\ T < (T_m - \Delta T) \end{cases} \quad (11)$$

wall of the crucible. At the rotation axis, the radial velocity is set to zero; this condition allows flow in the tangential z direction of the boundary but not in the normal r direction.

2.3 Computing details

The governing equations of the model were solved using the finite element method as provided by the commercial software COMSOL in the application modes *General Heat Transfer*, *Incompressible Navier-Stokes*, and [19]. For the stabilization of the solution of Navier-Stokes equations we have used a combination of GLS streamline diffusion and crosswind diffusion methods. We have used triangular mesh elements with adaptive mesh refinement. The number of triangular elements was different, depending on the type of simulation: in the most demanding conditions we start with about 20,000 triangular elements and after applying the adaptive refinement procedure the mesh consists of about 370,000 elements and about 730,000 degrees of freedom.

A three steps procedure was applied for finding the solution in the steady state simulations: i) first, we solved the problem on the default mesh; ii) then we used the adaptive solver to adapt the mesh; iii) finally, we used the parametric solver to decrease the value of ΔT (the half width of the mushy region) from a quite large value (30 – 40 K) down to 2 K. The final solution of such a stationary procedure can eventually be used as an initial condition for a transient simulation.

Different kinds of thermal initial conditions were tested: a uniform temperature in the entire domain of simulation ($T_0 = 0$ or $T_0 = T_m$ = melting point temperature), or a distribution like $T_0 = T_{ext}(z; t = 0)$, where T_{ext} is given by Eq. (1), or a previously calculated temperature field when transient simulations are considered. For velocity and pressure the initial conditions were $\mathbf{u}_0 = \mathbf{0}$ and $p = 0$ respectively.

The convergence is reached in less than 50 iteration (in most of the stationary cases in about 10 iterations). The computing time was from about 3 min for steady state thermal simulations (without flow) to about 70 min when the flow was taken into consideration and the three steps procedure described previously is applied (finding solution on default mesh + adapt the mesh + parametric decreasing of ΔT). For the transient simulations, when all the governing equations must be solved simultaneously, the computing time was about 60 min for 300 s of real time simulations.

All the calculations were done on a simple PC with dual core processor at 3.6 GHz and with 4 GB RAM.

2.4 Properties used in the computation

In our simulations we have used as charge materials CaF_2 and InSb respectively. The physical properties of

CaF_2 are obtained from Ref. [16], and those of InSb from Ref. [20]. They are listed in Table 1 together with the properties of the crucible materials.

Table 1. Physical properties of the materials used in simulations.

Property	CaF_2			InSb		
	Solid	Liquid	Crucible	Solid	Liquid	Crucible
Melting temperature T_m , K	1696			800		
Latent heat of solidification L , J/kg	3.8×10^5			2.01×10^5		
Thermal conductivity k , W/m K	6.0	0.6	28	4.57	9.23	2.68
Specific heat C_p , J/kg K	890	890	800	260.42	262.75	1052
Thermal expansion β , 1/K		2.682×10^{-4}			3.0×10^{-4}	
Density ρ , kg/m ³	3180	2594	2600	5760	6470	2200
Dynamic viscosity η , Pa·s		2.413×10^{-2}			1.94×10^{-3}	

3. Numerical results and discussions

In order to check the capabilities of the model described in the previous sections we performed stationary and transient simulations, using CaF_2 and InSb as charge materials. We have chosen the two materials for our simulations because, in our thermal conditions, the solid-melt interface for CaF_2 is convex, while for InSb it is concave, when seen from the melt. As usual, the solid-melt interface is represented by the melting point isotherm. The interface deflection f is defined as the difference between the interface location on the axis and at the inner wall of the crucible, $f = |z(0, t) - z(R_i, t)|$, where R_i is the inner radius of the crucible.

3.1 Steady state simulation

In a first set of simulations we have observed the changes of the solidification interface due to the convection in the melt for a stationary thermal distribution applied on the outer wall of the crucible, given by Eq. (1), with $v_{pulling} = 0$, $z_0 = 0.04$ m and $\Delta z = 0.01$ m, 0.02 m, 0.03 m, and 0.04 m respectively. The temperatures of the cold and hot zones of the furnace are $T_{inf} = 1650$ K and $T_{sup} = 1750$ K for CaF_2 simulations; when using InSb we have taken $T_{inf} = 750$ K and $T_{sup} = 850$ K, respectively. This gives rise to the same values of the thermal gradients for the two charge materials, $\delta_T = 50.0$ Kcm⁻¹, 25.0 Kcm⁻¹, 16.66 Kcm⁻¹, and 12.5 Kcm⁻¹ respectively. The first three values of these thermal gradients are larger than the values usually used in Bridgman systems but in this study we only intend to check the capabilities of the model and not to provide a quantitative validation of it.

Figs. 2.(a) – (b) shows the solid-melt interface without flow and with flow for CaF_2 and InSb respectively, when using the thermal gradient $\delta_T = 12.5$ Kcm⁻¹. In these figures we recognize the well known fact that the convection in the melt flattens the solid-melt interface. When using the other three thermal gradients the effect on the solidification interface is similar. The values of the

interface deflection for all the thermal gradients, together with the corresponding maximum velocities in the melt, are presented in Table 2. These results show that the thermal boundary conditions (i.e. thermal gradients) used in these simulations have a weak effect on the interface deflection.

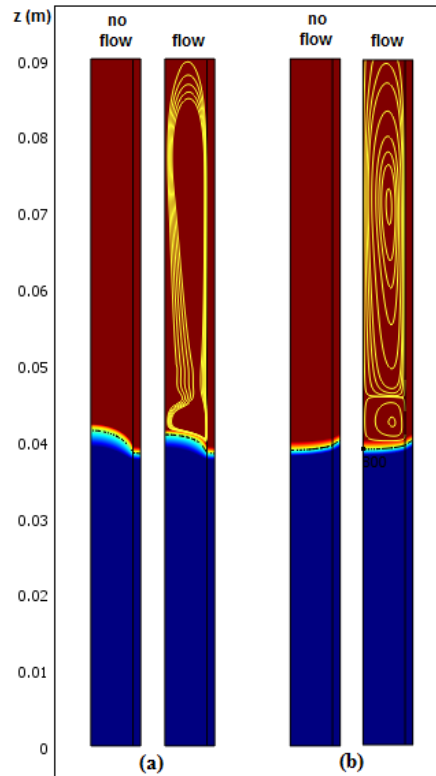


Fig. 2. Solid - melt interface for CaF_2 (a) and InSb (b), without and with flow, for $\delta_T = 12.5$ Kcm⁻¹ (color legend: blue = solid; red = liquid; rainbow = mushy zone).

As was pointed out by Crochet et al. [9], Lan et al. [15], and Boiton et al. [9], the maximum velocity of the

flow in the melt varies nearly *linearly* with respect to the interface deflection. The results of Boiton et al. [9] refers to the solidification of GaSb in a vertical Bridgman furnace and in a series of transient state simulations these authors obtained a *linear increase* of the maximum velocity with respect to the interface deflection. GaSb has similar physical properties to InSb, and the solidification

interface in the study of Boiton et al. was also concave, like in our simulations when using InSb. Apparently, our results for InSb indicate a similar linear increase of the maximum velocity of the flow with the interface deflection but this conclusion could be an exaggeration because the values of the interface deflection are very close to each other

Table 2. Interface deflection and maximum velocity versus thermal gradient for the steady state simulations.

Convection	Thermal gradient (Kcm ⁻¹)	CaF ₂		InSb	
		Interface deflection (mm)	Maximum velocity (ms ⁻¹)	Interface deflection (mm)	Maximum velocity (ms ⁻¹)
No	50.0	3.38	-	0.69	-
No	25.0	3.12	-	0.66	-
No	16.6	3.01	-	0.65	-
No	12.5	2.91	-	0.64	-
Yes	50.0	2.3	0.49 x 10 ⁻³	0.63	2.05 x 10 ⁻³
Yes	25.0	2.4	0.34 x 10 ⁻³	0.56	1.65 x 10 ⁻³
Yes	16.6	2.5	0.25 x 10 ⁻³	0.55	1.30 x 10 ⁻³
Yes	12.5	2.5	0.19 x 10 ⁻³	0.54	1.03 x 10 ⁻³

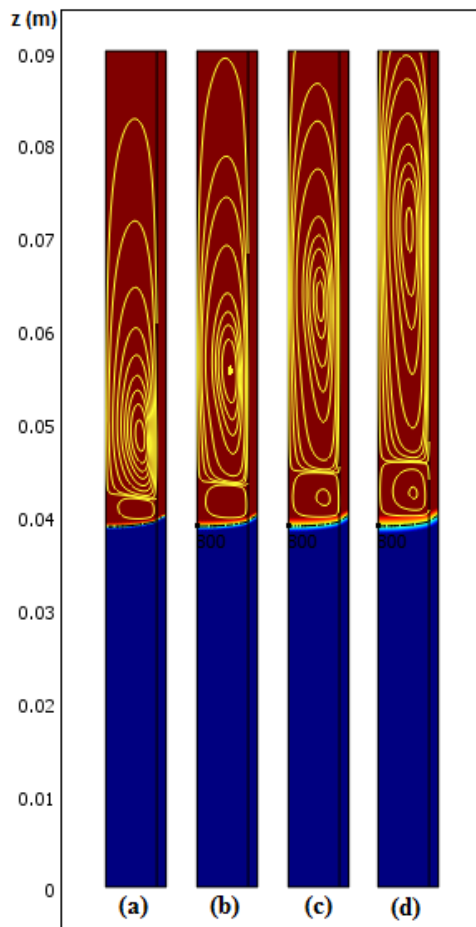


Fig. 3. Solid-melt interface for InSb, with flow, for $\delta_T = 50.0 \text{ Kcm}^{-1}$ (a), 25.0 Kcm^{-1} (b), 16.66 Kcm^{-1} (c), and 12.5 Kcm^{-1} (d).

In the case of the CaF₂ charge, the interface deflection has larger values than those obtained for InSb and the maximum velocity of the flow seems to *decrease nearly linearly* with respect to interface deflection. But, once again, we cannot say at this moment that this conclusion is a right one because the values of the interface deflection are very close to each other. We can say with certainty that the maximum velocity of the flow is decreasing when the thermal gradient is decreasing by using a symmetric enlargement of the adiabatic zone (fixed z_0 and larger Δz). At the same time, for large thermal gradients the center of the flow cell is close to the solidification interface; by decreasing the thermal gradient the center of the flow cell is moving away from the solidification interface (Fig. 3). This conclusion is restricted to our idealized model and cannot be extrapolated to real Bridgman furnaces; in real furnaces the thermal gradients and the position of the adiabatic zone are changed in an asymmetric manner by using crucible holders of different geometries and / or moving screens.

In a second set of steady state simulations we have used only InSb as charge material and one single value for Δz , namely $\Delta z = 0.01 \text{ m}$, but we changed the temperatures of the cold and hot zones of the furnace. These two temperatures can be changed symmetrically with respect to the melting point temperature of the charge material (i.e. T_{inf} is decreased and T_{sup} is increased with the same amount, such that $T_m - T_{inf} = T_{sup} - T_m$), or asymmetrically (i.e. $T_m - T_{inf} \neq T_{sup} - T_m$). Some results obtained in the symmetrical case are presented in Table 3. It seems that using our model the interface deflection remains practically unchanged when the axial thermal gradient becomes larger than about 50 Kcm^{-1} . Nevertheless, the axial profiles of the flow velocity in the melt show an increase of the maximum velocity in the two flow cells with the thermal gradient; moreover, the main maximum velocity changes its position and shifts upwards (its z coordinate increases) (Fig. 4).

Table 3. Interface deflection and maximum velocity of the flow in the melt for symmetrical changes of the cold and hot zones temperatures.

Δz (m)	T_m (K)	T_{inf} (K)	T_{sup} (K)	Thermal gradient (Kcm^{-1})	Interface deflection (mm)	Maximum velocity (ms^{-1})
0.01	800	600	1000	200	0.67	2.17×10^{-3}
		700	900	100	0.67	2.15×10^{-3}
		750	850	50	0.63	2.05×10^{-3}
		780	820	20	0.62	1.7×10^{-3}

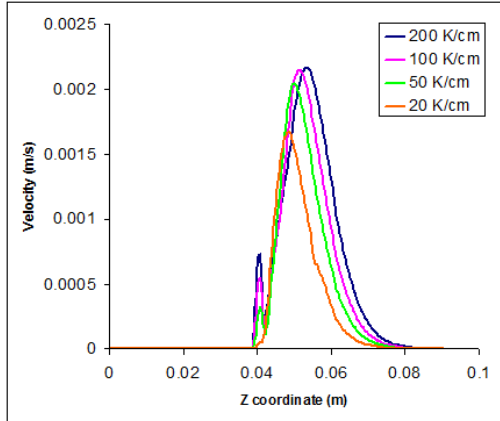


Fig. 4. Velocity profile in the melt as a function of the z coordinate for the same thermal gradients as in Table 3.

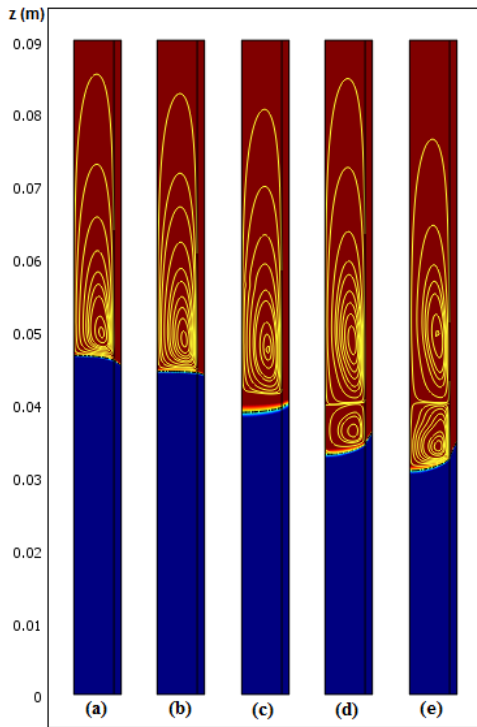


Fig. 5. Solid-melt interface for InSb, with flow, for asymmetrical changes of the cold and hot zones temperatures: (a) $T_{inf} = 600$ K, $T_{sup} = 820$ K; (b) $T_{inf} = 700$ K, $T_{sup} = 820$ K; (c) $T_{inf} = 780$ K, $T_{sup} = 820$ K; (d) $T_{inf} = 780$ K, $T_{sup} = 900$ K; (e) $T_{inf} = 780$ K, $T_{sup} = 1000$ K.

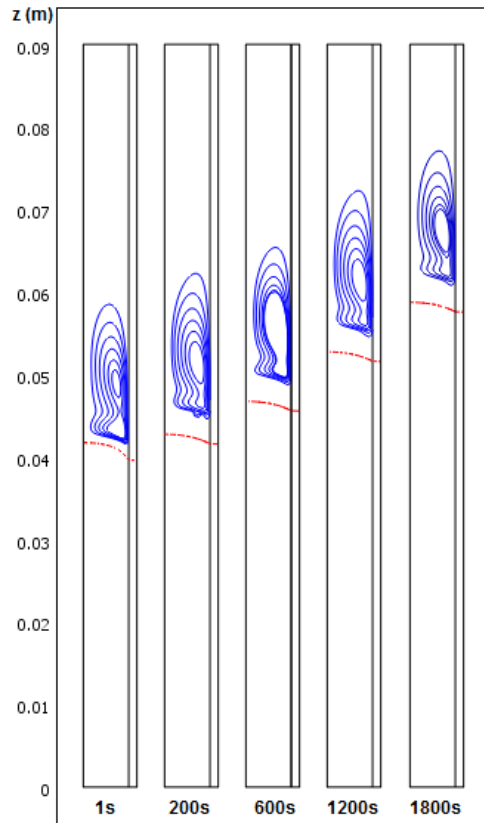
Fig. 5 presents the results obtained by varying asymmetrically the temperatures of the cold and hot zones of the furnace. For a given value of the temperature in the hot zone but not very far from the temperature of the melting point T_m there is a threshold value $T_{inf,lim}$ such that for $T_{inf} < T_{inf,lim}$ the interface is convex, and for $T_{inf} > T_{inf,lim}$ the interface is concave. If the temperature of the cold zone is not far below the temperature of the melting point and we increase the temperature of the hot zone, the solidification interface remains concave but its deflection changes from small to large values. In the same time, the asymmetric variation of the temperatures in the cold and hot zones has an important influence on the position of the solidification interface and the dimensions of the two flow cells, as seen in Figure 5. We can understand these features if we have in mind that lowering T_{inf} , for example, but keeping unchanged the form (width) of the thermal distribution $T_{ext}(z,t)$ the position of the melting point temperature T_m in this thermal profile shifts upwards. Consequently, the solidification interface position with respect to the symmetric thermal distribution shift upward as well. Interestingly, as seen from Fig. 5.(a) – (e), the flow cells system changes when passing from a concave solidification interface to a convex one: the lower flow cell disappears above flat or convex interfaces. Our results are in agreement with those reported by other authors (see, for example, Lan et al. [15]) and show that the axial thermal distribution on the outer boundary of the ampoule is a key factor to interface control.

3.2 Transient state simulations

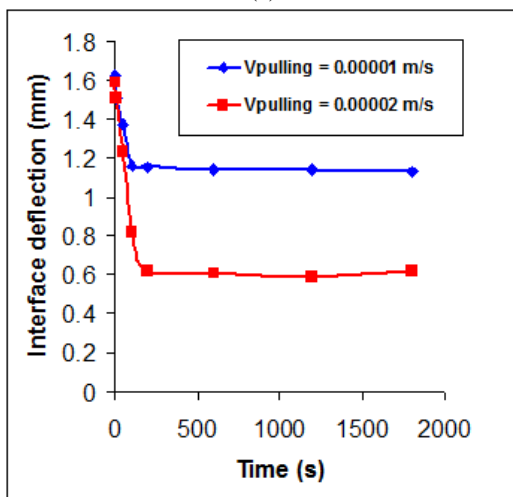
In order to demonstrate the effect of growth speed on the solid – melt interface we performed a series of transient state simulations.

Figs. 6.(a) – (b) show the dynamic evolution of the interface deflection in the case of CaF_2 for two different pulling rates, $v_{pulling} = 10 \times 10^{-6}$ m/s and 20×10^{-6} m/s respectively; the other constants in the thermal profile given by Eq. (1) are: $z_0 = 0.04$ m, $\Delta z = 0.01$ m, $T_{inf} = 1650$ K and $T_{sup} = 1750$ K. The initial conditions are obtained by setting a stationary thermal distribution on the outer wall of the crucible, $T_{ext}(z; t = 0)$. It is interesting to note that, in both cases, a constant interface deflection is reached after about 100 s for $v_{pulling} = 10 \times 10^{-6}$ m/s and respectively 200 s for $v_{pulling} = 20 \times 10^{-6}$ m/s. Moreover, the interface deflection for $v_{pulling} = 20 \times 10^{-6}$ m/s is about half of that obtained for $v_{pulling} = 10 \times 10^{-6}$ m/s. At the same time, as shown in Fig. 6(a), the flow cell in the melt does not

change its shape in time and the maximum velocity value remains at about 1.6×10^{-4} m/s for $v_{pulling} = 10 \times 10^{-6}$ m/s and respectively 1.35×10^{-4} m/s for $v_{pulling} = 20 \times 10^{-6}$ m/s. These observations allow us to say that a near steady-state operation can be obtained in a very short time from the beginning of the pulling.



(a)



(b)

Fig. 6. Effect of the pulling velocity on the interface deflection of CaF_2 : (a) snapshots with solid-melt interface and flow cell; (b) interface deflection vs. time for two pulling velocities.

Similar results, not shown here, are obtained with our model when the charge material is InSb and the interface is slightly concave. In this case the interface deflection increases very little, from about 0.63 mm at $t = 0$ to about 0.68 mm in the steady-state that is reached after about 600 s, when using the growth rate $v_{pulling} = 10 \times 10^{-6}$ m/s. Due to the small variation of the interface deflection, we have not observed a significant change with time of the shape of the flow cells in the melt, even for the case of InSb.

4. Conclusions

We have performed a local modeling of the solidification of CaF_2 and InSb in an idealized vertical Bridgman configuration. The thermal field in the system and the flow in the melt were calculated by performing steady-state and transient simulations. From the calculations presented in our paper it follows that during the solidification process the interface shape changes with relation to the variations of the thermal boundary conditions seen by the crucible. Changing the relative position of the solidification interface by decreasing the cold zone temperature or by increasing the hot zone temperature is very effective for interface shape control. The interface shape can be also be changed by varying the growth speed (pulling rate) and this fact can be helpful for obtaining a near steady-state operation with a nearly flat or slightly convex interface.

A further step in this study will be to incorporate in the model the internal radiation in the crystal and the heat transfer by convection and radiation from the system to the ambient. After that we will be able to compare the results of the simulations with those obtained in some crystal growth experiments and to optimize the heat transfer in real vertical Bridgman systems.

Acknowledgements

This work was supported by a grant of the European Social Fund through the Sectorial Operational Program for Human Resources Development, Project no. POSDRU/159/1.5/S/137750 coordinated by the University "A.I. Cuza" Iasi in partnership with the West University of Timisoara, and by the Project POSDRU/174/1.3/S/149155. The authors would like also to acknowledge Prof. Dr. D. Vizman and Assoc. Prof. Dr. F. Barvinschi for useful discussions.

References

- [1] V. R. Voller, C. Prakash, Int. J. Heat Mass Transfer **30**, 1709 (1987).
- [2] M. Jurisch, S. Eichler, M. Bruder, Vertical Bridgman Growth of Binary Compound Semiconductors, Chapter 9 in Handbook of Crystal Growth, Second Edition, Volume II, Part A, Ed. Peter Rudolph, Elsevier, Amsterdam, 2015, p. 331.

- [3] M.J. Crochet, F. Dupret, Y. Ryckmans, F.T. Geyling, E.M. Monberg, *J. Crystal Growth* **97**, 173 (1989).
- [4] S. Brandon, J.J. Derby, *J. Crystal Growth* **110**, 481 (1991).
- [5] S. Brandon, J.J. Derby, *J. Crystal Growth* **121**, 473 (1992).
- [6] S. Brandon, J.J. Derby, *J. Crystal Growth* **132**, 261 (1993).
- [7] D. Vizman, I. Nicoara, D. Nicoara, *J. Crystal Growth* **169**, 161 (1996).
- [8] F. Barvinschi, I. Nicoara, J.L. Santailier, T. Duffar, *Modelling Simul. Mater. Sci. Eng.* **6**, 691 (1998).
- [9] P. Boiton, N. Giacometti, J.L. Santailier, T. Duffar, J.P. Nabot, *J. Crystal Growth* **194**, 43 (1998).
- [10] R.A. Brown, D.H. Kim, *J. Crystal Growth* **109**, 50 (1991).
- [11] D.H. Kim, R.A. Brown, *J. Crystal Growth* **109**, 66 (1991).
- [12] D. Hofmann, T. Jung, G. Muller, *J. Crystal Growth* **128**, 213 (1993).
- [13] T. Suzuki, Y. Okano, K. Hoshikawa, T. Fukuda, *J. Crystal Growth* **128**, 435 (1993).
- [14] F. Barvinschi, O. Bunoiau, I. Nicoara, D. Nicoara, J.L. Santailier, T. Duffar, *J. Crystal Growth* **237-239**, 1762 (2002).
- [15] C. W. Lan, C.C. Ting, *J. Crystal Growth* **149**, 175 (1995).
- [16] H.B. Xiong, Y. Ma, L.L. Zheng, *J. Crystal Growth* **299**, 404 (2007).
- [17] P. Barvinschi, F. Barvinschi, *Proc. Physics Conference Tim-10, AIP Conference Proceedings Volume 1387*, 2011, p. 190.
- [18] T. L. Marin, *Proc. COMSOL Users Conference*, Boston, 2006.
- [19] COMSOL Multiphysics Model Library, COMSOL AB (2008).
- [20] S.-M. Epure, PhD Thesis, Grenoble, France (2011).

*Corresponding author: pc_barvi@yahoo.fr